ACS APPLIED MATERIALS & INTERFACES

www.acsami.org

Research Article

Self-Assembly of Silica–Gold Core–Shell Microparticles by Electric Fields Toward Dynamically Tunable Metamaterials

Han Gao,[§] Yihao Xu,[§] Kan Yao, and Yongmin Liu*

Cite This: *ACS Appl. Mater. Interfaces* 2021, 13, 14417–14422

Read Online

ACCESS | Metrics & More | Article Recommendations | Supporting Information

ABSTRACT: Metamaterials, rationally engineered composite materials with exotic properties, have provided unprecedented opportunities to manipulate the propagation of electromagnetic waves and control light–matter interactions in a prescribed manner. At present, most metamaterials are in solid states, and their functions are fixed once fabricated. Applying external electric fields to assemble metallic and metallodielectric particles into distinct configurations is an approach to realize dynamically tunable or reconfigurable metamaterials. In this paper, we show that core–shell microparticles can be self-assembled into chain structures under an alternating current (AC) electric field at different oscillation frequencies. We have conducted optical characterizations of silica–gold core–shell particles by Fourier transform infrared (FTIR) spectroscopy, which show distinct optical responses at mid-infrared wavelengths before and after the chain formation. Full-wave simulations unveil that the spectral features arise from the coupling between the sophisticated plasmonic resonant modes of individual core–shell particles. The reconfigurable metamaterials based on the manipulation and assembly of metallic and metallodielectric particles have potential applications in optofluidic devices, liquid-borne microcircuits, and optical sensing.

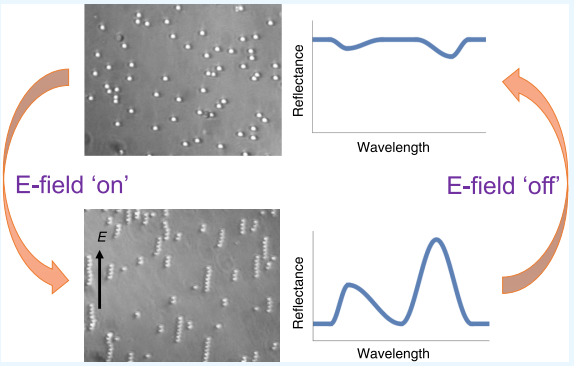

KEYWORDS: *tunable metamaterial, core–shell microparticle, self-assembly, AC electric field, infrared*

INTRODUCTION

Over the past decades, metamaterials have attracted extensive attention for their ability to control light propagation based on judiciously designed structures.[1−4] Metamaterials have enabled many novel optical properties, phenomena, and applications, including negative refractive indices,[5] strong chirality for twisting light,[6] superlenses and hyperlenses for sub-diffraction-limit imaging,[7−9] and invisibility cloaks.[10−12] The recently developed planar, two-dimensional metamaterials, known as metasurfaces, have become an emerging frontier in the metamaterial research.[13−15] These new designs are compatible with planar, low-cost manufacturing, and particularly suitable for device integration. However, conventional metamaterials and metasurfaces are mostly fabricated by top-down micro-/nanomanufacturing techniques and in the solid phase, making them very difficult to be reconfigured to perform different functions.

There is a pressing need put forward by the community to control metamaterials in situ and on demand to achieve dynamically tunable responses.[16,17] Over the past years, researchers have developed different approaches toward this goal, which can be categorized into two general strategies. The first strategy is to change the structural configuration of metamaterials by mechanical stretching and folding[18,19] or using micro-electromechanical system (MEMS) techniques[20,21] since the responses of metamaterials strongly depend on the geometry and arrangement of the building blocks. The second is to apply external stimuli, including light,[22] electric,[23−28] and magnetic fields,[29,30] heat,[31] as well as chemicals,[32] to modulate the optical properties of the constituent materials. For example, Wang et al. demonstrated optically reconfigurable metamaterials and photonic devices based on phase-change materials.[22] By changing the Fermi energy of graphene via a bias voltage, people have realized tunable metamaterials in the terahertz and infrared regions.[23−26]

In this paper, using self-assembled metallodielectric particles controlled by external alternating current (AC) fields, we realize reconfigurable metamaterials at infrared wavelengths. External stimuli such as electric fields,[33,34] shear,[35] gravity,[36] magnetic fields,[37−39] and light[40] have been widely used in colloidal assembly processes. Among these external fields, applying electric fields is probably the most mature and practical method. Electric-field-induced assembly can be accurately controlled by a

Received: February 8, 2021
Accepted: March 8, 2021
Published: March 17, 2021

https://dx.doi.org/10.1021/acsami.1c02724
ACS Appl. Mater. Interfaces 2021, 13, 14417–14422

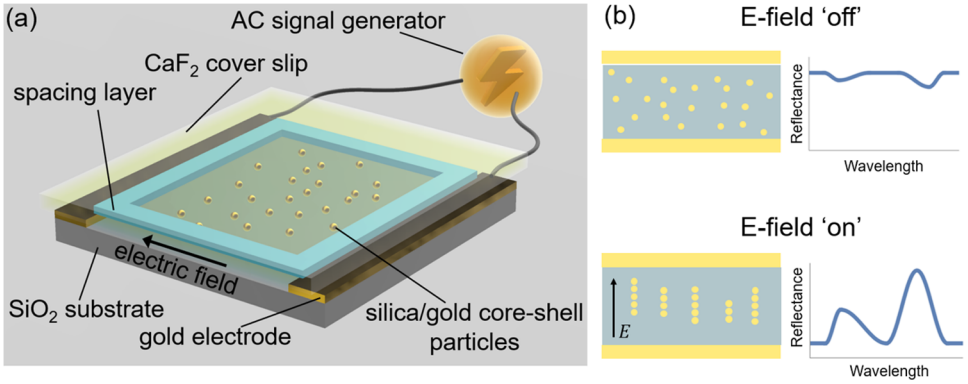

Figure 1. (a) Illustration of the experimental setup. (b) Schematic of colloidal configuration when an external electric field is turned off or on. The effect can be used to realize electrically tunable metamaterials.

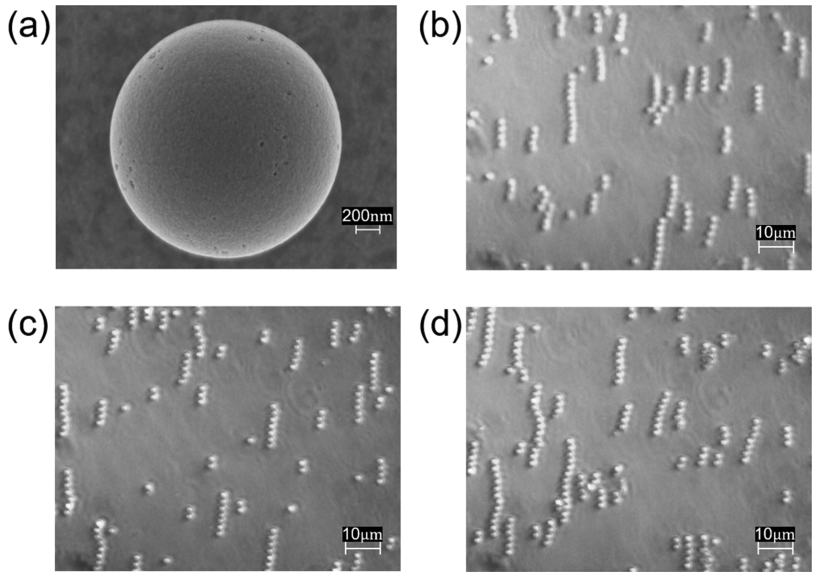

Figure 2. (a) SEM image of synthesized silica−gold core−shell particles. (b−d) Optical microscope images of the chain structures, when the frequency of the AC electric field is 10 Hz (b), 300 Hz, (c) and 100 kHz (d), respectively.

wide range of parameters, including the magnitude, frequency, and wave shape of the field. It has also be applied to self-propel on-chip sensors via microfabrication.[41] The manipulation of electric fields can result in different self-assembled structures. Randomly dispersed symmetric dielectric particles fully coated with gold in varying thicknesses behave distinctly under an AC electric field,[42−44] while some asymmetric dielectric colloids can also form unusual microstructures when they are subjected to an AC electric field.[45,46] Additionally, the aggregation orientation of uncoated particles preforms differently in response to a direct current (DC) electric field and an AC electric field.[47,48]

Although particle assembly under the control of the AC electric field has been well studied, the dynamic optical responses of the assembled structures are largely unexplored, impeding the further development and application of electrically tunable optical metamaterials in the aqueous environment. Here, we investigate the infrared optical responses of silica−gold core−shell particles by Fourier transform infrared (FTIR) spectroscopy when the AC electric fields are absent and present. Our experimental and numerical studies show that four resonant modes appear upon the formation of chain structures. To the best of our knowledge, our work is the first demonstration of reconfigurable metamaterials at infrared wavelengths through self-assembly of metallodielectric particles controlled by external AC fields. It may lead to a new class of soft metamaterials, which will attract the attention of researchers from different disciplines, such as optics, metamaterials, colloidal assembly, and microfluidics. Our research paves a new way toward electrically tunable metamaterials, which may be used as functionalized carriers for ultrasensitive infrared absorption spectroscopy,[49,50] catalysis or drug delivery,[51,52] microactuators and microsensors in MEMS devices,[53] and particles separations in microfludic devices.[54]

EXPERIMENTAL DESIGNS

In the present work, we apply AC electric fields on silica−gold core−shell microparticles in solution to form chain structures. The optical spectrum measurement is conducted in situ by FTIR. Previously, the spectrum measurements of chain structures were conducted when particles are stabilized on a substrate after the fluid in the suspension evaporated.[55−57] The difficulties of measuring the optical responses of particles in a suspension are attributed to the following issues: (1) The absorption of infrared light by water is significant, leading to a relatively weak signal-to-noise ratio. (2) Particles undergo random Brownian motion in a fluid; hence, measuring a single

https://dx.doi.org/10.1021/acsami.1c02724
ACS Appl. Mater. Interfaces 2021, 13, 14417−14422

particle or chain in solution is challenging. (3) Water evaporation changes the thickness of the water layer in the system, affecting the FTIR spectra of the chain structures.

Keeping these problems in mind, we have designed an experimental setup as shown in Figure 1a. The AC-field-induced assembly of microparticles was performed in a setup with coplanar parallel electrodes. A droplet of core−shell particle suspension was injected into a sealed cell, consisting of the glass substrate, a 6-μm-thick polymer spacing layer, and a calcium fluoride (CaF_2) window on the top. CaF_2 is nearly transparent in almost the entire mid-infrared wavelength range of our interest (>90% transmittance from 0.2 to 7 μm). Therefore, it was placed on the top of the cell to serve as the transparent window for the incoming light. The CaF_2 window can also help to substantially slow down the water evaporation, leading to more stabilized particle assembly. This allows us to increase the scan times from 200 to 500 during the FTIR measurement, which greatly improves the signal-to-noise ratio, especially when polarizers are used in the measurement. With the confinement of the polymer spacer, the core−shell particle suspension can form a thin film between the CaF_2 window and the glass substrate. When an AC electric field with a frequency ranging from 40 Hz to 1 MHz is applied parallel to the substrate, the dispersed particles self-assemble into chain structures, as illustrated in Figure 1b. Importantly, the system can be reversed back to dispersed particles by a low-frequency (1 Hz) AC electric field that lasts for 1−3 s. As a result, the optical responses of the aqueous metamaterials can be dynamically controlled.

RESULTS AND DISCUSSION

Figure 2a shows the scanning electron microscope (SEM) image of a silica−gold core−shell particle that we synthesized. We can see a smooth and uniform surface of the core−shell particle. The silica−gold core−shell particles were chemically synthesized based on the protocol reported by Brinson et al.[58] with slight modification.[53] The surfaces of 2 μm silica beads were decorated with 3-aminopropyltriethoxysilane (APTES) and 1−2 nm gold ions were attached gradually on the modified surface of silica beads. The synthesis details are given in the Materials and Methods section. According to the gold ion to silica bead ratio and additional inspection using high-magnification SEM (Figure S1), the gold shell thickness was estimated to be 10−13 nm.

AC electric fields with a 10 V peak-to-peak voltage and frequencies ranging from 10 Hz to 1 MHz were applied to the core−shell particles in solution to form chain structures based on the charge electrophoresis force.[53,59] The motion and field-induced assembly of the particles were observed using an optical microscope coupled to the FTIR spectrometer. Figure 2b−d presents the formed chain structures under the AC electric field with frequencies of 10 Hz, 300 Hz, and 100 kHz, respectively. The dynamic assembly and disassembly processes of core−shell particles are shown in Supporting Information Video S1 and Figure S2. Though stable chain structures could form across a wide range of frequencies, the reasons causing the formation of chain structures are different. Dielectrophoresis (DEP) force and induced-charge electro-osmosis (ICEO) are the two major causes. DEP is the movement of particles in a nonuniform electric field. ICEO flow refers to fluid flow around a polarizable surface. The applied AC electric field causes the inhomogeneous distribution of polarization charges on the surface, giving rise to the formation of a volumetric distribution of ionic charge density near it.[60] Both DEP force and ICEO flow are frequency-dependent.[61] At low frequencies (e.g., 10 Hz), the AC electric field can be regarded as nearly static and there is no field in the bulk electrolyte. Therefore, the magnitude of the ICEO flow tends to be zero while the DEP force is constant and dominantly induces the assembly of particles. According to the permittivity of water and gold, the DEP force exerted on the particles is a positive DEP (p-DEP) force.[59] With the increase of frequency (300 Hz), the ICEO effect occurs accompanied by p-DEP force, resulting in the chain structure assemblies. When the frequency reaches 10 kHz, the frequency is too high, so that there is insufficient time for the induced charge to form in the double layer. As a result, the ICEO flow tends to be zero again. Besides, at this frequency, the polarizability of the particle might be identical to the suspending medium. In this case, there is no induced dipole, and the DEP force becomes zero. Consequently, around 10 kHz, no chain structures can be retained under Brownian motion. With the continuous increase of frequency to 100 kHz, particles are assembled into chain configurations again due to the negative-DEP (n-DEP) force. It is because at this frequency, lacking insufficient responding time, ICEO flow is still zero, and the dielectric constant of the water is much higher than that of silica−gold core−shell nanoparticles. The distribution of dispersive core−shell particles subject to AC fields at 10 kHz and 1 MHz is shown in Figure S3.

FTIR measurements were conducted in situ for the formed chains under both s-polarized (perpendicular to the chains) and p-polarized (parallel to the chains) incidence. In our experiment, the samples were fixed on the sample stage of the FTIR microscope, while the polarizer was rotated to achieve the appropriate polarized light. As plotted in Figure 3a, the

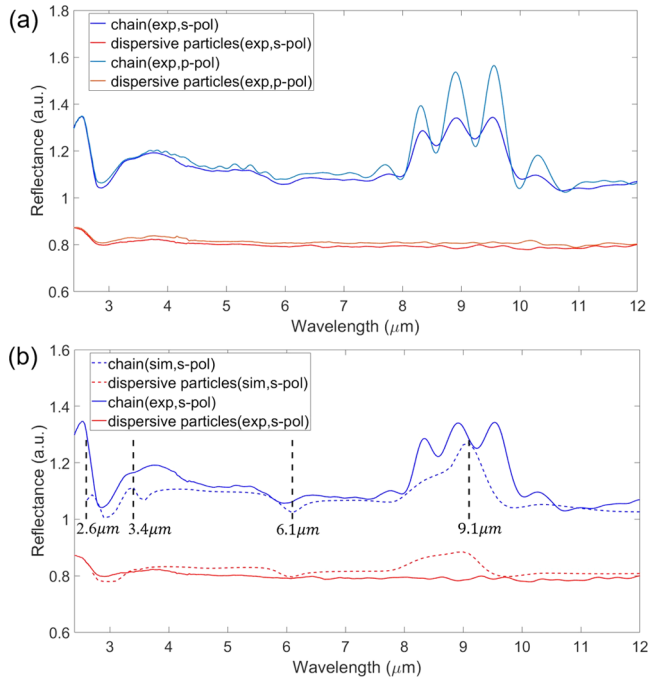

Figure 3. (a) Measured FTIR spectra for 2 μm silica−gold core−shell particles with different structures and incident polarizations. Blue: chain structures under s-polarized light. Light blue: chain structures under p-polarized light. Red: dispersed particles under s-polarized light. Orange: dispersed particles under p-polarized light. (b) Measured (solid line) and simulated (dashed line) FTIR spectra for 2 μm core−shell particles in different configurations when the normal incidence light is s-polarized. The main resonant wavelengths are labeled for the chain structures.

https://dx.doi.org/10.1021/acsami.1c02724
ACS Appl. Mater. Interfaces 2021, 13, 14417−14422

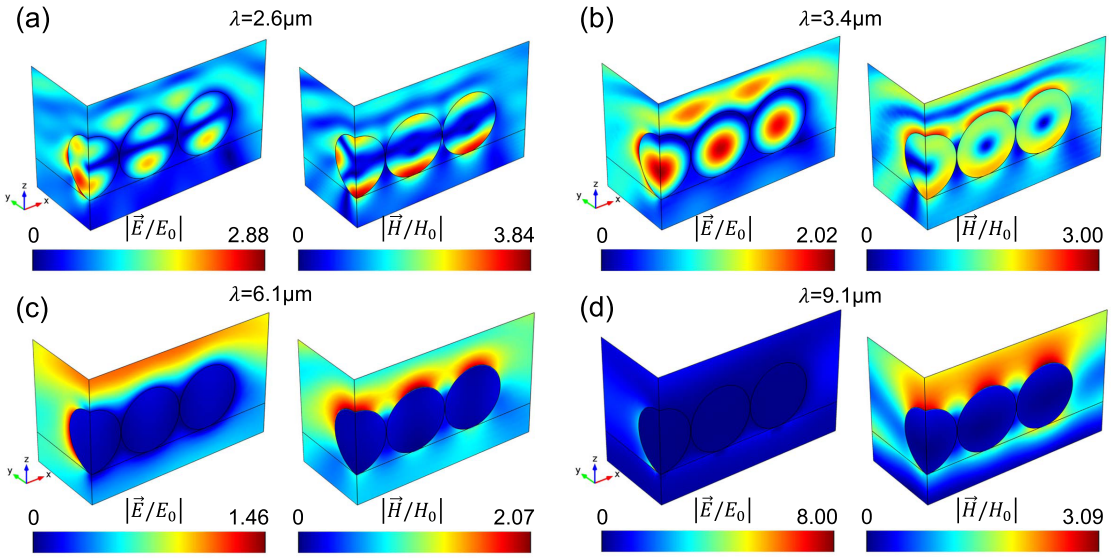

Figure 4. Simulated electric field and magnetic field (normalized to incident wave) of the silica−gold core−shell chain at different resonance wavelengths. The field distributions manifest four resonant modes: (a) electric quadrupole mode ($\lambda = 2.6\ \mu$m), (b) electric dipole mode $\lambda = 3.4\ \mu$m, (c) Au−water plasmonic mode ($\lambda = 6.1\ \mu$m), and (d) Au−silica gap plasmonic mode ($\lambda = 9.1\ \mu$m).

resonance features for the chain structures are rather different in comparison with dispersed particles. For dispersed particles, the spectra are very similar for both polarizations, because the particles are isotropic. However, the spectra show distinct differences for chains. Specifically, the reflectivity of chains subjected to p-polarized light is slightly stronger than that of s-polarized light. The reason is that stronger scattering of plasmonic modes occurs when the electric field is along the particle chain for p-polarized light. There are also several specific resonances that appeared at a longer wavelength around 8−10 μm.

To further confirm these spectral features, we have performed numerical simulations using the commercial electromagnetic solver COMSOL Multiphysics. In the simulations, the permittivity of silica was taken from Kischkat et al.,[62] and the permittivity of gold was taken from the data of Rakić et al.[63] The simulation results of the chain (of five core−shell particles) structure subjected to s-polarized normal incidence agree reasonably well with the experimental results, although there is a slight red shift. As illustrated in Figure 3b, the randomly dispersed particles show a quite flat spectrum with only a small peak at around 9.1 μm. However, this feature was not observed in experiments. The possible reason is the random position of individual particles, which causes the scattered waves from individual particles to cancel with each other. In contrast, the situation is very different for chain structure, where the relative positions of particles are determined within each chain structure, indicated by the peaks and dips in both the measured and simulated spectra. The simulated spectrum for p-polarized normal incidence shows similar features but with stronger amplitude in comparison with s-polarization incidence, which is consistent with the FTIR measurement. These results are further discussed in the Supporting Information (Figure S4). The separation distance between adjacent particles in the chain was set as 10 nm in the simulation, while we proved that the simulated spectra are not sensitive to this setting, as discussed in the Supporting Information (see Table S1 and Figure S5).

To understand the origin of the spectral features, in Figure 4a−d, we plot the electric and magnetic fields at the resonant wavelengths. From the simulation result, we observe a quadrupole at $\lambda = 2.6\ \mu$m indicated by the two intensity lobes along the half perimeter in the plot of the field in particle, which can be seen more clearly in Figure S6 in the Supporting Information. At $\lambda = 3.4\ \mu$m, the electric dipole resonance of the SiO_2 core is dominant, performing like a cavity and producing a peak in the reflectance spectrum. The electric field confinement at the interface between water and particle surface led to the appearance of resonance modes at $\lambda = 6.1\ \mu$m. For the reflectivity peak centered around $\lambda = 9.1\ \mu$m, we can clearly observe that the field is concentrated on the bottom of the particles. It is related to the highly lossy nature of silica substrate between 7.8 and 10 μm. Especially near 9.1 μm, where the permittivity of silica is negative, the substrate becomes metal-like and we have Au−silica gap plasmon mode at this wavelength. All of these results are consistent with our previous work.[57]

CONCLUSIONS

In summary, we experimentally demonstrated electric-field-induced self-assembly of core−shell microparticles and conducted in situ spectroscopic measurement. Silica−gold core−shell with high uniformity were synthesized by a chemical method. Colloidal could self-assemble into chain configurations under applied external AC electric field, and the optical properties change before and after the assembly of clusters. The four resonant modes of the chain structures shown in the FTIR spectra are in good agreement with the simulation results. The external electric field control makes it feasible and convenient to create promising dynamically tunable metamaterials, which hold potential applications in various disciplines including miniaturized photonic circuits, biosensors, and DNA detecting probes.

MATERIALS AND METHODS

Preparation of Core−Shell Microparticles. Silica beads (2 μm) were first washed carefully to remove unwanted stabilization groups on their surface and then redispersed in ethanol of equal volume. After that, the surface of silica beads

https://dx.doi.org/10.1021/acsami.1c02724
ACS Appl. Mater. Interfaces 2021, 13, 14417−14422

was modified by APTES. Based on the protocol developed by Brinson et al.,[58] 1−2 nm gold nanoparticles were prepared and attached to the surface of the modified silica beads by the electrostatic force. These gold nanoparticles served as nucleation sites for the later shell formation. Subsequently, aged chloroauric acid planting solution was mixed with silica particles. Under rapid stirring, formaldehyde was added to the mixture to conduct the reduction of gold ions. With the continuous reduction of gold ions in the planting solution, the attached gold nanoparticles increased in size, coalesced, and finally formed a complete gold shell on silica cores.

Electrode Fabrication. The coplanar parallel electrodes were made by depositing 5 nm titanium as an adhesion layer and 40 nm gold on a 2.5 cm × 2.5 cm glass substrate.[64] A Kapton tape with a width of 1 mm was placed at the center of the glass substrate to act as a mask. After the metal deposition, the tape was removed, and a 1 mm wide channel between the electrodes was created. The wire bonding was made with UV glue and silver paint. UV glue was used for bonding the wires on the electrodes, while the silver paint could improve the electrical conductivity between the electrodes and wires. The wires were subsequently connected to an AC field generator, which provided external AC electric fields to induce colloidal assembly.

■ ASSOCIATED CONTENT

Supporting Information

The Supporting Information is available free of charge at https://pubs.acs.org/doi/10.1021/acsami.1c02724.

(1) characterization of core−shell microparticle, (2) dynamic assembly and disassembly of core−shell particles, (3) simulation of the optical spectra of chain structures, (4) effect of the separation distance between particles in the chain structure, and (5) field distribution of the quadruple mode (PDF)

Dynamic assembly and disassembly process of core-shell particles by controlling the external AC electric field (Video S1) (MP4)

■ AUTHOR INFORMATION

Corresponding Author

Yongmin Liu − *Department of Electrical and Computer Engineering and Department of Mechanical and Industrial Engineering, Northeastern University, Boston, Massachusetts 02115, United States;* orcid.org/0000-0003-1084-6651; Email: y.liu@northeastern.edu

Authors

Han Gao − *Department of Electrical and Computer Engineering, Northeastern University, Boston, Massachusetts 02115, United States*

Yihao Xu − *Department of Mechanical and Industrial Engineering, Northeastern University, Boston, Massachusetts 02115, United States*

Kan Yao − *Department of Electrical and Computer Engineering, Northeastern University, Boston, Massachusetts 02115, United States;* orcid.org/0000-0002-9144-2618

Complete contact information is available at: https://pubs.acs.org/10.1021/acsami.1c02724

Author Contributions

[§]H.G. and Y.X. contributed equally to this work.

Notes

The authors declare no competing financial interest.

■ ACKNOWLEDGMENTS

We acknowledge the financial support from the Office of Naval Research (N00014-16-1-2409) and the National Science Foundation (CBET-1931777) .

■ REFERENCES

(1) Smith, D. R.; Pendry, J. B.; Wiltshire, M. C. Metamaterials and Negative Refractive Index. *Science* **2004**, *305*, 788−792.

(2) Soukoulis, C. M.; Wegener, M. Past Achievements and Future Challenges in the Development of Three-dimensional Photonic Metamaterials. *Nat. Photonics* **2011**, *5*, 523−530.

(3) Liu, Y.; Zhang, X. Metamaterials: A New Frontier of Science and Technology. *Chem. Soc. Rev.* **2011**, *40*, 2494−2507.

(4) Cai, W.; Shalaev, V. M. *Optical Metamaterials*; Springer, 2010.

(5) Shelby, R. A.; Smith, D. R.; Schultz, S. Experimental Verification of a Negative Index of Refraction. *Science* **2001**, *292*, 77−79.

(6) Gansel, J. K.; Thiel, M.; Rill, M. S.; Decker, M.; Bade, K.; Saile, V.; von Freymann, G.; Linden, S.; Wegener, M. Gold Helix Photonic Metamaterial as Broadband Circular Polarizer. *Science* **2009**, *325*, 1513−1515.

(7) Liu, Z.; Lee, H.; Xiong, Y.; Sun, C.; Zhang, X. J. s. Far-field Optical Hyperlens Magnifying Sub-diffraction-limited Objects. *Science* **2007**, *315*, 1686.

(8) Fang, N.; Lee, H.; Sun, C.; Zhang, X. Sub−diffraction-limited Optical Imaging with a Silver Superlens. *Science* **2005**, *308*, 534−537.

(9) Pendry, J. B. Negative Refraction Makes a Perfect Lens. *Phys. Rev. Lett.* **2000**, *85*, 3966−3969.

(10) Liu, Y.; Zhang, X. Recent Advances in Transformation Optics. *Nanoscale* **2012**, *4*, 5277−5292.

(11) Pendry, J. B.; Schurig, D.; Smith, D. R. Controlling Electromagnetic Fields. *Science* **2006**, *312*, 1780−1782.

(12) Leonhardt, U. Optical Conformal Mapping. *Science* **2006**, *312*, 1777−1780.

(13) Yu, N.; Capasso, F. Flat Optics with Designer Metasurfaces. *Nat. Mater.* **2014**, *13*, 139−150.

(14) Yu, N.; Genevet, P.; Kats, M. A.; Aieta, F.; Tetienne, J.-P.; Capasso, F.; Gaburro, Z. Light Propagation with Phase Discontinuities: Generalized Laws of Reflection and Refraction. *Science* **2011**, *334*, 333−337.

(15) Kildishev, A. V.; Boltasseva, A.; Shalaev, V. M. Planar Photonics with Metasurfaces. *Science* **2013**, *339*, No. 1232009.

(16) Zheludev, N. I. Obtaining Optical Properties on Demand. *Science* **2015**, *348*, 973−974.

(17) Bang, S.; Kim, J.; Yoon, G.; Tanaka, T.; Rho, J. Recent Advances in Tunable and Reconfigurable Metamaterials. *Micromachines* **2018**, *9*, No. 560.

(18) Wang, Z.; Jing, L.; Yao, K.; Yang, Y.; Zheng, B.; Soukoulis, C. M.; Chen, H.; Liu, Y. Origami-based Reconfigurable Metamaterials for Tunable Chirality. *Adv. Mater.* **2017**, *29*, No. 1700412.

(19) Pryce, I. M.; Aydin, K.; Kelaita, Y. A.; Briggs, R. M.; Atwater, H. A. Highly Strained Compliant Optical Metamaterials with Large Frequency Tunability. *Nano Lett.* **2010**, *10*, 4222−4227.

(20) Kan, T.; Isozaki, A.; Kanda, N.; Nemoto, N.; Konishi, K.; Takahashi, H.; Kuwata-Gonokami, M.; Matsumoto, K.; Shimoyama, I. Enantiomeric Switching of Chiral Metamaterial for Terahertz Polarization Modulation Employing Vertically Deformable MEMS Spirals. *Nat. Commun.* **2015**, *6*, No. 8422.

(21) Ou, J.-Y.; Plum, E.; Zhang, J.; Zheludev, N. I. An Electromechanically Reconfigurable Plasmonic Metamaterial Operating in the Near-infrared. *Nat. Nanotechnol.* **2013**, *8*, 252−255.

(22) Wang, Q.; Rogers, E. T.; Gholipour, B.; Wang, C.-M.; Yuan, G.; Teng, J.; Zheludev, N. I. Optically Reconfigurable Metasurfaces and Photonic Devices based on Phase Change Materials. *Nat. Photonics* **2016**, *10*, 60−65.

(23) Ma, W.; Huang, Z.; Bai, X.; Zhan, P.; Liu, Y. Dual-band Light Focusing Using Stacked Graphene Metasurfaces. *ACS Photonics* **2017**, *4*, 1770−1775.
(24) Ju, L.; Geng, B.; Horng, J.; Girit, C.; Martin, M.; Hao, Z.; Bechtel, H. A.; Liang, X.; Zettl, A.; Shen, Y. R. Graphene Plasmonics for Tunable Terahertz Metamaterials. *Nat. Nanotechnol.* **2011**, *6*, 630−634.
(25) Yan, H.; Li, X.; Chandra, B.; Tulevski, G.; Wu, Y.; Freitag, M.; Zhu, W.; Avouris, P.; Xia, F. N. Tunable Infrared Plasmonic Devices Using Graphene/Insulator Stacks. *Nat. Nanotechnol.* **2012**, *7*, 330−334.
(26) Lee, S. H.; Choi, M.; Kim, T.-T.; Lee, S.; Liu, M.; Yin, X.; Choi, H. K.; Lee, S. S.; Choi, C.-G.; Choi, S.-Y. Switching Terahertz Waves with Gate-controlled Active Graphene Metamaterials. *Nat. Mater.* **2012**, *11*, 936−941.
(27) Park, S.; Lee, G.; Park, B.; Seo, Y.; bin Park, C.; Chun, Y. T.; Joo, C.; Rho, J.; Kim, J. M.; Hone, J. J. L. S. Electrically Focus-tuneable Ultrathin Lens for High-resolution Square Subpixels. *Light: Sci. Appl.* **2020**, *9*, No. 98.
(28) Kim, I.; Yun, J.; Badloe, T.; Park, H.; Seo, T.; Yang, Y.; Kim, J.; Chung, Y.; Rho, J. Structural Color Switching with a Doped Indium-gallium-zinc-oxide Semiconductor. *Photonics Res.* **2020**, *8*, 1381−1387.
(29) Valente, J.; Plum, E.; Youngs, I. J.; Zheludev, N. I. Nano-and Micro-Auxetic Plasmonic Materials. *Adv. Mater.* **2016**, *28*, 5176−5180.
(30) Lapine, M.; Shadrivov, I. V.; Powell, D. A.; Kivshar, Y. S. Magnetoelastic Metamaterials. *Nat. Mater.* **2012**, *11*, 30−33.
(31) Ou, J.-Y.; Plum, E.; Jiang, L.; Zheludev, N. Reconfigurable Photonic Metamaterials. *Nano Lett.* **2011**, *11*, 2142−2144.
(32) Fontana, J.; Nita, R.; Charipar, N.; Naciri, J.; Park, K.; Dunkelberger, A.; Owrutsky, J.; Piqué, A.; Vaia, R.; Ratna, B. Widely Tunable Infrared Plasmonic Nanoantennas Using Directed Assembly. *Adv. Opt. Mater.* **2017**, *5*, No. 1700335.
(33) Shah, A. A.; Ganesan, M.; Jocz, J.; Solomon, M. J. Direct Current Electric Field Assembly of Colloidal Crystals Displaying Reversible Structural Color. *ACS Nano* **2014**, *8*, 8095−8103.
(34) Wen, T.; Zhang, W.; Liu, S.; Hu, A.; Zhao, J.; Ye, Y.; Chen, Y.; Qiu, C.-W.; Gong, Q.; Lu, G. J. S. A. Steering Valley-polarized Emission of Monolayer MoS2 Sandwiched in Plasmonic Antennas. *Sci. Adv.* **2020**, *6*, No. eaao0019.
(35) Ackerson, B. J. Shear Induced Order and Shear Processing of Model Hard Sphere Suspensions. *J. Rheol.* **1990**, *34*, 553−590.
(36) Davis, K.; Russel, W.; Glantschnig, W. Disorder-to-order Transition in Settling Suspensions of Colloidal Silica: X-ray Measurements. *Science* **1989**, *245*, 507−510.
(37) Haghgooie, R.; Li, C.; Doyle, P. S. Experimental Study of Structure and Dynamics in a Monolayer of Paramagnetic Colloids Confined by Parallel Hard Walls. *Langmuir* **2006**, *22*, 3601−3605.
(38) Helseth, L.; Wen, H.; Hansen, R.; Johansen, T.; Heinig, P.; Fischer, T. Assembling and Manipulating Two-dimensional Colloidal Crystals with Movable Nanomagnets. *Langmuir* **2004**, *20*, 7323−7332.
(39) Fernandez-Rodriguez, M. A.; Grillo, F.; Alvarez, L.; Rathlef, M.; Buttinoni, I.; Volpe, G.; Isa, L. Feedback-controlled Active Brownian Colloids with Space-dependent Rotational Dynamics. *Nat. Commun.* **2020**, *11*, No. 4223.
(40) Korda, P. T.; Grier, D. G. Annealing Thin Colloidal Crystals with Optical Gradient Forces. *J. Chem. Phys.* **2001**, *114*, 7570−7573.
(41) Juárez, J. J.; Feicht, S. E.; Bevan, M. A. Electric Field Mediated Assembly of Three Dimensional Equilibrium Colloidal Crystals. *Soft Matter* **2012**, *8*, 94−103.
(42) Zhang, L.; Zhu, Y. J. L. Directed Assembly of Janus Particles under High Frequency AC-electric Fields: Effects of Medium Conductivity and Colloidal Surface Chemistry. *Langmuir* **2012**, *28*, 13201−13207.
(43) Liu, W.; Wang, C.; Ding, H.; Shao, J.; Ding, Y. AC Electric Field Induced Dielectrophoretic Assembly Behavior of Gold Nanoparticles in a Wide Frequency Range. *Appl. Surf. Sci.* **2016**, *370*, 184−192.
(44) Gangwal, S.; Pawar, A.; Kretzschmar, I.; Velev, O. D. Programmed Assembly of Metallodielectric Patchy Particles in External AC Electric Fields. *Soft Matter* **2010**, *6*, 1413−1418.
(45) Ma, F.; Wang, S.; Wu, D. T.; Wu, N. Electric-field−induced Assembly and Propulsion of Chiral Colloidal Clusters. *Proc. Natl. Acad. Sci. U.S.A.* **2015**, *112*, 6307−6312.
(46) Heatley, K. L.; Ma, F.; Wu, N. Colloidal Molecules Assembled from Binary Spheres under an AC Electric Field. *Soft Matter* **2017**, *13*, 436−444.
(47) Genevet, P.; Yu, N.; Aieta, F.; Lin, J.; Kats, M. A.; Blanchard, R.; Scully, M. O.; Gaburro, Z.; Capasso, F. Ultra-thin Plasmonic Optical Vortex Plate based on Phase Discontinuities. *Appl. Phys. Lett.* **2012**, *100*, No. 013101.
(48) Gong, J.; Wu, N. Electric-field Assisted Assembly of Colloidal Particles into Ordered Nonclose-packed Arrays. *Langmuir* **2017**, *33*, 5769−5776.
(49) Adato, R.; Altug, H. In situ Ultra-sensitive Infrared Absorption Spectroscopy of Biomolecule Interactions in Real Time with Plasmonic Nanoantennas. *Nat. Commun.* **2013**, *4*, No. 2154.
(50) Rodrigo, D.; Limaj, O.; Janner, D.; Etezadi, D.; De Abajo, F. J. G.; Pruneri, V.; Altug, H. Mid-infrared Plasmonic Biosensing with Graphene. *Science* **2015**, *349*, 165−168.
(51) Roh, K.-H.; Martin, D. C.; Lahann, J. Biphasic Janus Particles with Nanoscale Anisotropy. *Nat. Mater.* **2005**, *4*, 759−763.
(52) Wu, Y.; Fu, A.; Yossifon, G. Active Particles as Mobile Microelectrodes for Selective Bacteria Electroporation and Transport. *Sci. Adv.* **2020**, *6*, No. eaay4412.
(53) Gangwal, S.; Cayre, O. J.; Bazant, M. Z.; Velev, O. D. Induced-charge Electrophoresis of Metallodielectric Particles. *Phys. Rev. Lett.* **2008**, *100*, No. 058302.
(54) Sajeesh, P.; Sen, A. K. J. M. Particle Separation and Sorting in Microfluidic Devices: A Review. *Microfluid. Nanofluid.* **2014**, *17*, 1−52.
(55) Fan, J. A.; Bao, K.; Wu, C.; Bao, J.; Bardhan, R.; Halas, N. J.; Manoharan, V. N.; Shvets, G.; Nordlander, P.; Capasso, F. Fano-like Interference in Self-assembled Plasmonic Quadrumer Clusters. *Nano Lett.* **2010**, *10*, 4680−4685.
(56) Yan, J.; Liu, P.; Lin, Z.; Wang, H.; Chen, H.; Wang, C.; Yang, G. W. Magnetically Induced Forward Scattering at Visible Wavelengths in Silicon Nanosphere Oligomers. *Nat. Commun.* **2015**, *6*, No. 7042.
(57) Yao, K.; Liu, Y. Infrared Plasmonic Resonators based on Self-assembled Core−shell Particles. *ACS Photonics* **2018**, *5*, 844−851.
(58) Brinson, B. E.; Lassiter, J. B.; Levin, C. S.; Bardhan, R.; Mirin, N.; Halas, N. J. Nanoshells Made Easy: Improving Au Layer Growth on Nanoparticle Surfaces. *Langmuir* **2008**, *24*, 14166−14171.
(59) Velev, O. D.; Bhatt, K. H. On-chip Micromanipulation and Assembly of Colloidal Particles by Electric Fields. *Soft Matter* **2006**, *2*, 738−750.
(60) Feng, H.; Chang, H.; Zhong, X.; Wong, T. N. Recent Advancement in Induced-charge Electrokinetic Phenomena and Their Micro-and Nano-fluidic Applications. *Adv. Colloid Interface Sci.* **2020**, *280*, No. 102159.
(61) Ren, Y.; Liu, W.; Jia, Y.; Tao, Y.; Shao, J.; Ding, Y.; Jiang, H. Induced-charge Electroosmotic Trapping of Particles. *Lab Chip* **2015**, *15*, 2181−2191.
(62) Kischkat, J.; Peters, S.; Gruska, B.; Semtsiv, M.; Chashnikova, M.; Klinkmüller, M.; Fedosenko, O.; Machulik, S.; Aleksandrova, A.; Monastyrskyi, G.; Flores, Y.; Masselink, W. T. Mid-infrared Optical Properties of Thin films of Aluminum Oxide, Titanium Dioxide, Silicon Dioxide, Aluminum Nitride, and Silicon Nitride. *Appl. Opt.* **2012**, *51*, 6789−6798.
(63) Rakić, A. D.; Djurišić, A. B.; Elazar, J. M.; Majewski, M. L. Optical Properties of Metallic Films for Vertical-cavity Optoelectronic Devices. *Appl. Opt.* **1998**, *37*, 5271−5283.
(64) Shah, A. A.; Schultz, B.; Zhang, W.; Glotzer, S. C.; Solomon, M. J. Actuation of Shape-memory Colloidal Fibres of Janus Ellipsoids. *Nat. Mater.* **2015**, *14*, 117−124.

https://dx.doi.org/10.1021/acsami.1c02724
ACS Appl. Mater. Interfaces 2021, 13, 14417−14422